Model for drag forces in the crevice of piston gauges in the viscous-flow and molecular-flow regimes

J. W. Schmidt, S. A. Tison and C. D. Ehrlich

Abstract. A model for drag forces in the crevice of pneumatic piston gauges is presented. The model uses an interpolation function for momentum transfer between the piston and the cylinder mediated by the gas flowing in the crevice. The interpolation function bridges the gap between the molecular-flow and viscous-flow regimes, and is then used to develop an expression for the effective area of a piston gauge. The deviations of the effective area of this model from the viscous-flow results are derived for both floating-piston and floating-cylinder designs. Model results are compared with published measurements of the effective area of several piston gauges in which relative changes as large as 30×10^{-6} (30 ppm) were observed when different pressurizing gases were used.

1. Introduction

Piston gauge pressure generators have become one of the most reliable pressure standards in the world today in the range 20 kPa to 500 MPa. The Pressure and Vacuum Group at the National Institute of Standards and Technology (NIST) uses piston gauges as transfer standards to compare pressures from different primary standards and to distribute the pressure scale to other laboratories in the United States and throughout the world. One such transfer gauge, known within the NIST as PG-28 (a gas-operated/lubricated gauge), has served as the linchpin to anchor pressure calibrations at the NIST in the pressure range one atmosphere and above. Gauge PG-28 is most often used in gauge mode to transfer calibrations to other secondary gauges at the NIST and to the standards of other laboratories. However, its calibration has been based on an absolute-mode calibration against a mercury manometer primary standard [1]. To cover the jump to gauge-mode operation an additional 6×10^{-6} (1σ) relative uncertainty was included because of possible effects from unknown drag forces in the crevice [2]. The present model is an attempt to quantify the possible differences in effective area from a geometrical effective area and any differences when changing the operation from absolute to gauge mode.

In this model we extend a derivation developed previously [3] for azimuthal drag forces applied to spin-decay rate measurement to include vertical drag forces in the annular region (Section 2). The derivation has been used to interpret previous measurements of effective area using other gauges for two gases, helium and nitrogen [4]. The extended derivation of the drag force in the vertical direction begins with the viscous (or Poiseuille-flow) regime followed by the molecular-flow regime. The two results are then combined using an interpolating function to describe the drag forces in both regimes. The interpolating function for the drag force in the annular region is followed by an application of this result to an expression for the effective area of a piston gauge (Section 3). In Section 4 we compare the model with data obtained by Welch et al. [1] in gauge and absolute modes. They measured relative changes in the effective areas of several piston gauges and found changes as high as 30×10^{-6} (30 parts per million, or 30 ppm). The present model orders the changes in a predictable way based on the molecular weight and viscosity of the pressurizing gas.

2. Derivation of the drag force

2.1 Poiseuille-flow regime

The drag force in the Poiseuille-flow regime (i.e. the crevice width is much larger than the molecular mean free path) is given by

$$F_{\mathrm{d}} = A\eta \, \frac{\mathrm{d}v_z(z,r)}{\mathrm{d}r} \, |_{r=R_0}, \tag{1}$$

where A is the piston-cylinder overlap area $2\pi R_0 L$, η is the dynamic viscosity, r and z are the radial and axial coordinates, respectively, and $v_z(z,r)$ is the velocity

J. W. Schmidt, S. A. Tison[1] and C. D. Ehrlich[2]: Process Measurements Division, National Institute of Standards and Technology (NIST), Gaithersburg, MD 20899, USA.
1. Currently at Millipore Corp., Dallas, Texas; 2. Technical Standards Activities Program, NIST.

profile of the gas within the annular region [5],

$$v_z(z,r) = \frac{1}{4\eta}\frac{\mathrm{d}P(z)}{\mathrm{d}z}\times \left(R_1^2 - r^2 + \frac{(R_1^2 - R_0^2)}{\ln(R_1/R_0)}\ln(r/R_1)\right). \quad (2)$$

Here, $\mathrm{d}P/dz$ is the pressure gradient. The piston and cylinder radii are R_0 and R_1, respectively, and L is the length of the overlap area between piston and cylinder. The derivative of the velocity profile with respect to r is

$$\frac{\mathrm{d}v_z(z,r)}{\mathrm{d}r} = \frac{1}{4\eta}\frac{\mathrm{d}P(z)}{\mathrm{d}z}\times \left(-2r + \frac{(R_1^2 - R_0^2)}{\ln(R_1/R_0)}\frac{1}{r}\right). \quad (3)$$

If we define the annular width $h = R_1 - R_0$, then for small h/R_0, but not so small as to be in the molecular-flow regime,

$$\frac{\mathrm{d}v_z(z,r)}{\mathrm{d}r}|_{r=R_0} \approx \frac{1}{2\eta}\frac{\mathrm{d}P(z)}{\mathrm{d}z}(h), \approx \quad (4a)$$

$$\frac{6 < v(z) >}{h}. \quad (4b)$$

Equation (4b) was obtained by observing that the average flow velocity $< v_z(z) >$ at the axial coordinate z, is the integral of (2) over the annular area:

$$< v_z(z) > \approx \frac{h^2}{12\eta}\frac{\mathrm{d}P(z)}{\mathrm{d}z}. \quad (5)$$

The molecular flow through the annulus is

$$J = 2\pi R_0 h < v_z(z) > n(z). \quad (6)$$

Here, $n(z)$ is the molecular number density. After substituting (4b) into (1) and eliminating $< v_z(z) >$ with (6) we obtain

$$F_\mathrm{d} \approx \frac{6JL}{h^2 n(z)}\,\eta. \quad (7)$$

We finally note that η in (7) is approximately independent of pressure for the pressures near one atmosphere, while the analogous momentum transfer term to be developed in Section 2.2 for the molecular-flow regime is proportional to $n(z)$ and hence to the pressure.

2.2 Molecular-flow regime

In the molecular-flow regime the velocity profile is taken to be constant for a given z. The drag force on the piston in this regime (i.e. the crevice width is much smaller than the molecular mean free path) is equal to the average momentum transfer per molecular collision event multiplied by the number of events per second [6]:

$$F_\mathrm{d} \approx M < v(z) > Acn(z)/4. \quad (8a)$$

Here, M is the molecular mass, $Acn(z)/4$ is the number of molecule/wall collision events per second, A is the overlap area, $n(z)$ is the number density of the molecules, $c = (8kT/\pi M)^{1/2}$ is the mean molecular speed, k is Boltzmann's constant, and T is the temperature in kelvins. By combining (6) and (8a) we obtain

$$F_\mathrm{d} = \frac{MJcL}{4h} = \quad (8b)$$

$$\frac{6JL}{h^2 n(z)}\left(\frac{Mchn(z)}{24}\right). \quad (8c)$$

Equation (8c) was obtained by factoring out the same coefficients as appear before η in (7). The remaining quantities in parentheses act as a momentum transfer term analogous to viscosity in (7).

2.3 Interpolating function between regimes

The two limiting cases given by (7) and (8c) in the two regimes described above are rewritten below:

$$F_\mathrm{d} = \frac{6JL}{h^2 n(z)}\times$$

$$\left\{\begin{array}{lll} \eta & : \text{ viscous flow;} & \lambda < h \end{array}\right\} \quad (9a)$$

$$\left\{\begin{array}{lll} \dfrac{Mchn(z)}{24} & : \text{ molecular flow;} & \lambda > h \end{array}\right\}, \quad (9b)$$

where λ is the mean free path.

Next, we define an interpolating or momentum transfer function $F_3[P]$ to replace the separate quantities within the braces in (9a) and (9b) with a single function in exact parallel with similar momentum transfer functions F_1 and F_2 of [3]:

$$F_3[P(z)] \equiv \frac{\eta}{1 + \beta_3/P(z)}, \quad (10)$$

where $\beta_3 = 24\ \eta kT/Mch$ has been defined so that $F_3[P \to 0]$ matches smoothly with (9b).

With this definition for the interpolating function between the limiting behaviours given by (9a) and (9b), we can rewrite (9) as an integral over the elemental contributions $\delta L(= dz)$:

$$\delta F_\mathrm{d} = \frac{6J}{h^2}\frac{F_3[P(z)]}{n(z)}\,\mathrm{d}z, \quad (11)$$

and

$$F_\mathrm{d} = \frac{6J}{h^2}\int_0^L \frac{F_3[P(z)]}{n(z)}\,\mathrm{d}z. \quad (12)$$

We change variables from z to P and assume the simplest case, that of an ideal gas $P(z) = n(z)kT$. Since the present model pressure profile is the same

as that of [3] we use without derivation those results: $\mathrm{d}z = D(P+\beta_2)\mathrm{d}P/J\eta kT$, where $D = \pi h^3 R_0/6$, $\beta_2 = 64\eta kT/\pi M ch$, and

$$J = \frac{D}{\eta kTL}\left(\frac{P_1^2 - P_0^2}{2} + \beta_2(P_1 - P_0)\right). \quad (13)$$

With these substitutions (12) becomes

$$F_\mathrm{d} = \frac{6D}{h^2}\int_{P_0}^{P_1}\frac{P+\beta_2}{P+\beta_3}\,\mathrm{d}P, \quad (14)$$

which is easily integrated to give

$$F_\mathrm{d} = \frac{6D}{h^2}\,(P_1 - P_0 - (\beta_3 - \beta_2))\ln\left(\frac{P_1+\beta_3}{P_0+\beta_3}\right). \quad (15)$$

Thus we have the force F_d in terms of two pressures, P_0 and P_1 (the absolute pressures at the entrance and exit of the annular region), and the two molecular properties of the pressurizing gas, viscosity and molecular weight.

3. Effective areas predicted by the model

From the force F_d as described in Section 2 and given by (15), we can calculate the effective area, A_eff, as a function of P_0 and the differential pressure$P_1 - P_0$. The effective area predicted by the treatment above for a conventional floating-piston design (gas flows upwards) is

$$A_\mathrm{eff} \equiv \pi R_0^2 + F_\mathrm{d}/(P_1 - P_0), \equiv \quad (16a)$$

$$\pi R_0^2\left\{1 + \frac{h}{R_0}\times \left[1 - \frac{\beta_3 - \beta_2}{P_1 - P_0}\,\ln\left(\frac{P_1+\beta_3}{P_0+\beta_3}\right)\right]\right\}, \quad (16b)$$

and for a floating-cylinder design (gas flows downwards),

$$A_\mathrm{eff} \equiv \pi R_1^2 - F_\mathrm{d}/(P_1 - P_0), \equiv \quad (17a)$$

$$\pi R_1^2\left\{1 - \frac{h}{R_1}\times \left[1 - \frac{\beta_3 - \beta_2}{P_1 - P_0}\,\ln\left(\frac{P_1+\beta_3}{P_0+\beta_3}\right)\right]\right\}. \quad (17b)$$

A_eff depends on η (through β_2 and β_3), P_0 and P_1. These contributions to the effective area are in addition to any effects due to deformation of the piston or cylinder. Note that the viscous-flow result normally used retains only the term h/R_0 (or $-h/R_1$) and gives an effective area that is constant and independent of both gas species and mode of operation (i.e. independent of η and P_0):

$$A^*_\mathrm{eff} \equiv \pi R_0^2\left\{1 + \frac{h}{R_0}\right\}, \quad (18a)$$

and

$$A^*_\mathrm{eff} \equiv \pi R_1^2\left\{1 - \frac{h}{R_1}\right\}, \quad (18b)$$

where A^* is the viscous-flow effective area. Equations (18a) and (18b) refer to the conventional and floating-cylinder designs, respectively.

The relative differences between (17) and the baseline viscous-flow model ((18a) for a conventional floating-piston design) is

$$\frac{A_\mathrm{eff} - A^*_\mathrm{eff}}{A^*_\mathrm{eff}} = -\frac{h}{R_0}\,\frac{\beta_3 - \beta_2}{P_1 - P_0}\ln\left(\frac{P_1+\beta_3}{P_0+\beta_3}\right). \quad (19)$$

The lower portions of Figures 1 and 2 show the differences predicted by (19) for six different pressurizing gases: helium (He), nitrogen (N_2), carbon dioxide (CO_2), neon (Ne), argon (Ar) and krypton (Kr). One can see that in the absolute mode ($P_0 \sim 0$) large gas-species effects can occur. The lines plotted in the figures were generated from (19) in which the crevice width, h, was taken to be 3 μm and the piston radius, R_0, was taken to be 0.005 m. Large shifts in effective area can also occur between absolute and gauge modes.

Also included in the upper portions of Figures 1 and 2 are predictions for the same gases for a floating-cylinder design with $h = 1$ μm, $R_0 = 0.025$ m crevice width. Note (i) the sign change because the gas in the crevice is flowing downwards, and (ii) the scale factor change ($\times 10$).

4. Comparison of the model with experiment

We have compared the present model with measurements by Welch et al. [1, Table 1] in which they measured shifts in effective area of two piston gauges relative to the effective area obtained using helium. Welch et al. also used the same six gases: He, N_2, CO_2, Ne, Ar and Kr, and because they obtained their data using another piston gauge (PG-28) as a standard, we modelled both the test gauge and the standard gauge with (19). Figures 3 and 4 give data they obtained from one of these gauges (absolute and gauge modes, respectively). Note the large effect observed – about 30 ppm in the case of CO_2 in the absolute mode relative to helium.

Figures 5 and 6 show the deviations of their data (PG-30) from the present model. We modelled the standard that they used (PG-28) with the values $h = 0.7$ μm and $R_0 = 0.01$ m. In absolute mode the fitting procedure (a Marquardt-Levenburg non-linear algorithm) resulted in a value $h = (3.2 \pm 0.2)$ μm for one of the gauges (PG-30) and $h = (3.1 \pm 0.2)$ μm for the other (PG-31). Although these values appear to be too large for the gauges Welch et al. studied, the model at least orders the effective areas in the proper sequence with regard to the molecular properties (molecular weight and viscosity). In gauge mode a value of $h = (1.2 \pm 0.6)$ μm resulted. The fall rates measured

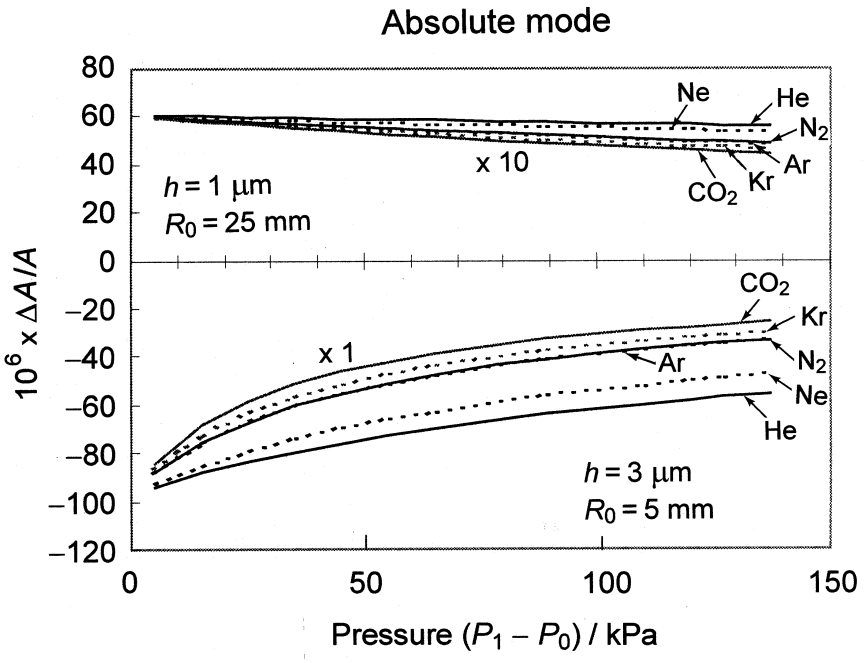

Figure 1. Differences in the absolute-mode effective area from the viscous-flow limit are displayed for two piston gauges. The plots below the axis represent a piston gauge with a conventional floating-piston design with $h = 3$ μm, $R_0 = 5$ mm. The plots above the axis represent a floating-cylinder design with $h = 1$ μm, $R_0 = 25$ mm. (Note scale change above axis.)

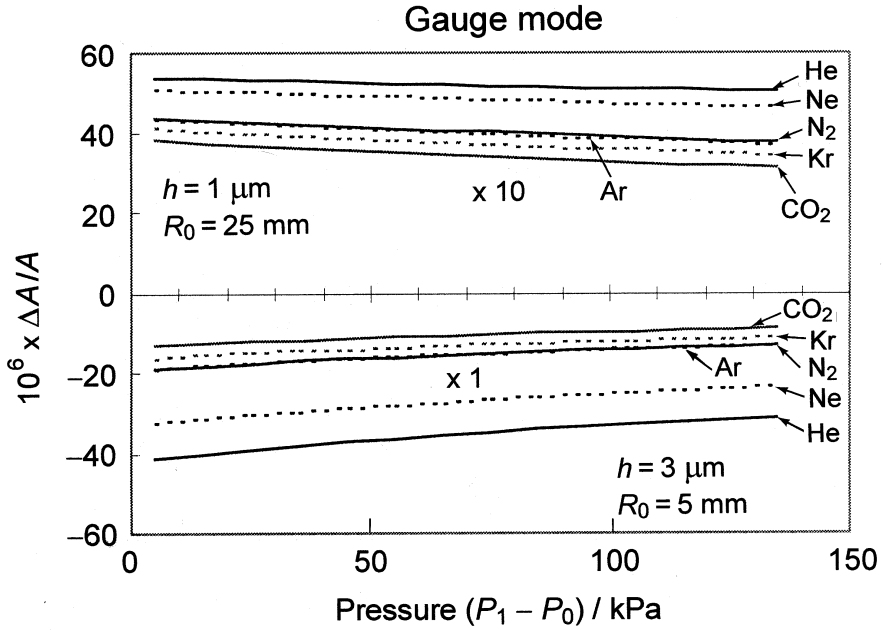

Figure 2. Differences in the gauge-mode effective area from the viscous-flow limit are displayed for two piston gauges. The plots below the axis represent a piston gauge with a conventional floating-piston design with $h = 3$ μm, $R_0 = 5$ mm. The plots above the axis represent a floating-cylinder design $h = 1$ μm, $R_0 = 25$ mm. (Note scale change above axis.)

by Welch et al. can also be used to estimate the crevice widths of PG-30 and PG-31. When this is done, values for h of 1.9 μm and 2.1 μm result for PG-30 and PG-31, respectively.

The present model shows promise in that it is able to obtain a good fit within 3 ppm to data that are initially divergent up to 30 ppm. Its shortcomings are that it could not fit the gauge- and absolute-mode data simultaneously and that it could not fit other data in the literature [2, 7]. Further research is needed to discover the source of the disagreement and to improve on the model.

With regard to the present model, we intend to extend it to allow for non-ideal crevice shapes, for example. The present model assumes perfect cylindricity for both piston and cylinder in addition

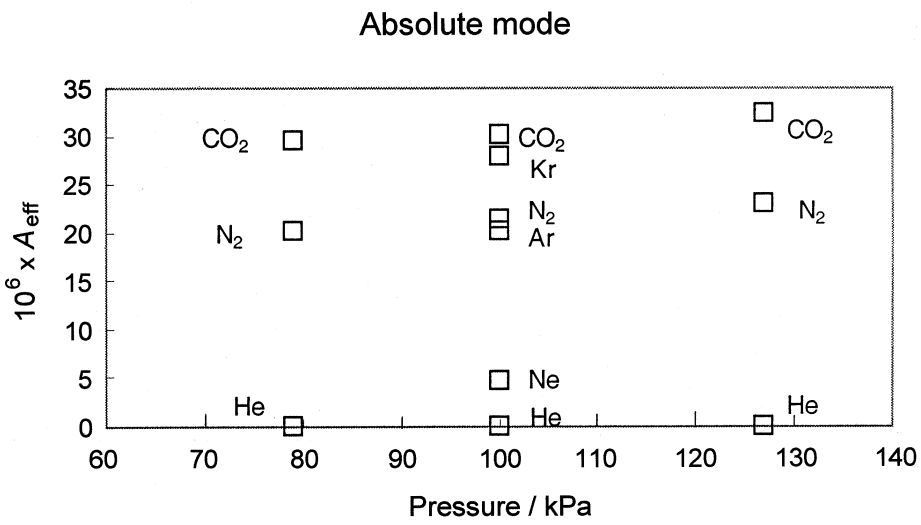

Figure 3. Changes in the absolute-mode effective area of a piston gauge from various gases used as the pressure fluid. The changes are relative to helium. The squares represent the data (PG-30) of Welch et al. [1], reproduced by permission of the authors.

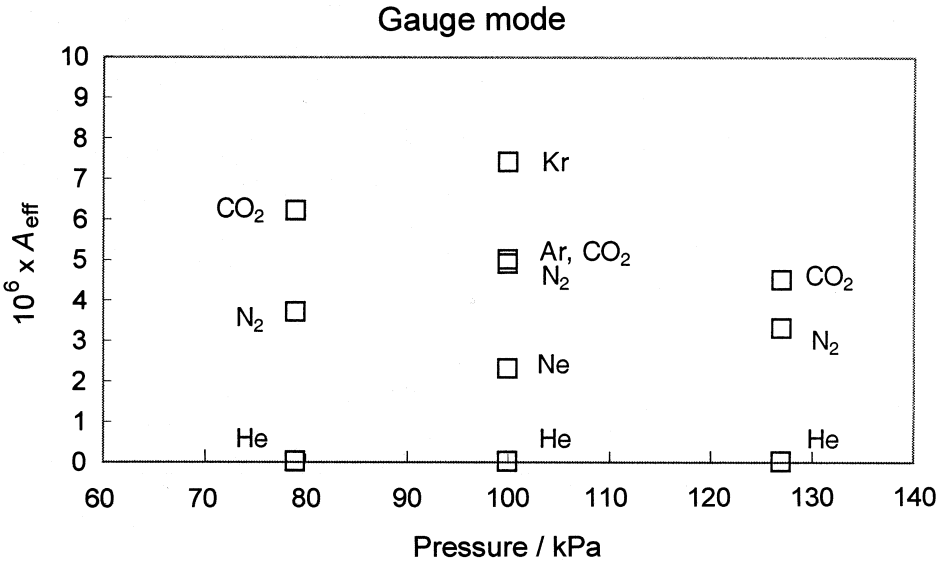

Figure 4. Changes in the gauge-mode effective area of a piston gauge from various gases used as the pressure fluid. The changes are relative to helium. The squares represent the data (PG-30) of Welch et al. [1], reproduced by permission of the authors.

to perfect alignment. With regard to the measurements, more high-quality data need to be gathered in other circumstances. Other gases that might provide useful information are hydrogen (H_2) and sulfur-hexafluoride (SF_6). These two gases have well-separated molecular weights and the viscosity of H_2 is less than half that of the other six gases used by Welch et al. They were used successfully in rotational decay rate measurements by Schmidt et al. [3]. Meyer and Reilly have also investigated A_{eff} in relation to six gases: H_2, ^3He, ^4He, N_2, CO_2 and SF_6 [7]. We have not fully analysed their data with the present model.

5. Conclusion

A model for the behaviour of pneumatic piston gauges has been presented which indicates that the effective area of piston gauges should vary in a predictable way with viscosity and the molecular weight of the pressurizing fluid. This model has been compared with the measurements of Welch et al. in both the absolute and gauge modes. The model provides a partial explanation for the large shifts in effective area observed by Welch et al. [1] and it explains the order of the shifts with gas species in both gauge and absolute modes. The

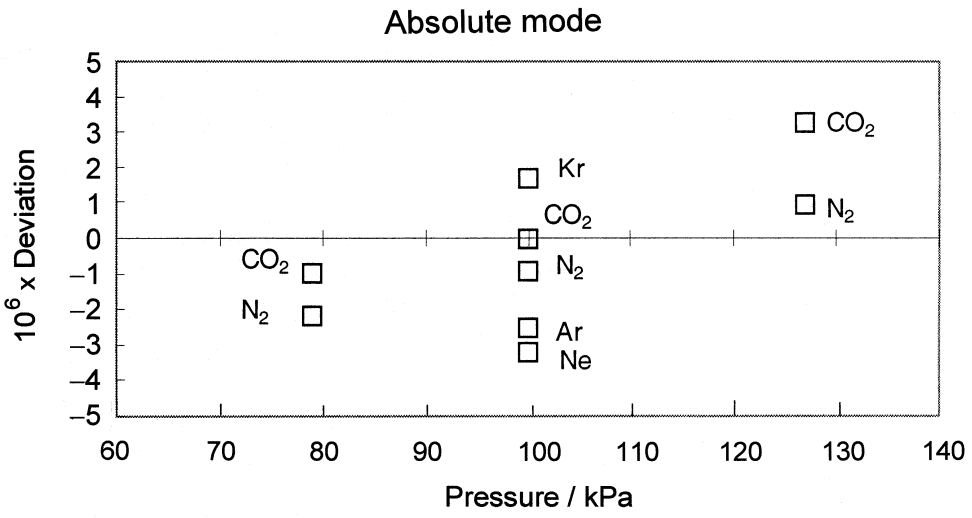

Figure 5. Residuals of a least-squares fit by the present model to the absolute-mode data of Welch et al. The crevice width, h, was used as the fitting parameter and a value of 3.2 μm resulted.

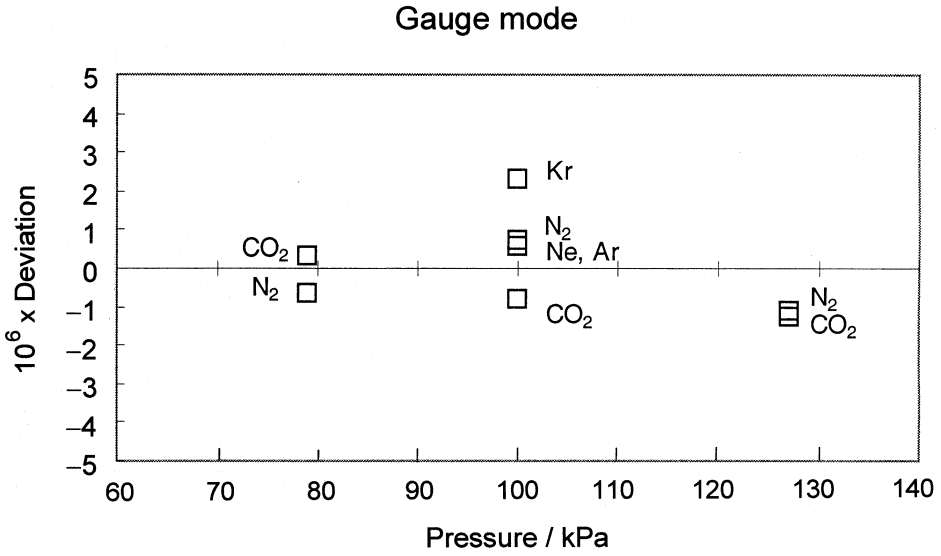

Figure 6. Residuals of a least-squares fit by the present model to the gauge-mode data of Welch et al. The crevice width, h, was used as the fitting parameter and a value of 1.2 μm resulted.

model is unable to explain the magnitude of the shift in effective area between gauge and absolute mode.

Acknowledgements. One of the authors (JWS) thanks Vern Bean for his critical reading of the typescript.

References

1. Welch B. E., Edsinger R. E., Bean V. E., Ehrlich C. D., High Pressure Metrology, *BIPM Monographie 89/1*, 1989, 81-94.
2. Tilford C. R., Hyland R. W., Yi-Tang S., High Pressure Metrology, *BIPM Monographie 89/1*, 1989, 105-123.
3. Schmidt J. W., Welch B. E., Ehrlich C. D., *Meas. Sci. Technol.*, 1993, **4**, 26-34.
4. Schmidt J. W., Welch B. E., Ehrlich C. D., *Metrologia*, 1993/94, **30**, 599-602.
5. Landau L. P., Lifshitz E. M., *Fluid Mechanics*, Vol. 6, London, Pergamon, 1959.
6. Sears F. W., *An Introduction to Thermodynamics, The Kinetic Theory of Gases and Statistical Mechanics*, Reading, Mass., Addison-Wesley, 1964.
7. Meyer C. W., Reilly M. L., *Metrologia*, 1993/94, **30**, 595-597.